buildings

MDPI

Article

Optimized Computational Intelligence Model for Estimating the Flexural Behavior of Composite Shear Walls

Masoomeh Mirrashid [1], Hosein Naderpour [1], Denise-Penelope N. Kontoni [2,3,*], Anna Jakubczyk-Gałczyńska [4], Robert Jankowski [4] and Tan N. Nguyen [5]

[1] Faculty of Civil Engineering, Semnan University, Semnan 35131-19111, Iran; m.mirrashid@semnan.ac.ir (M.M.); naderpour@semnan.ac.ir (H.N.)
[2] Department of Civil Engineering, School of Engineering, University of the Peloponnese, GR-26334 Patras, Greece
[3] School of Science and Technology, Hellenic Open University, GR-26335 Patras, Greece
[4] Faculty of Civil and Environmental Engineering, Gdansk University of Technology, 80-233 Gdansk, Poland; annjakub@pg.edu.pl (A.J.-G.); jankowr@pg.edu.pl (R.J.)
[5] Department of Architectural Engineering, Sejong University, 209 Neungdong-ro, Gwangjin-gu, Seoul 05006, Republic of Korea; tnnguyen@sejong.ac.kr
* Correspondence: kontoni@uop.gr

Abstract: This article presents a novel approach to estimate the flexural capacity of reinforced concrete-filled composite plate shear walls using an optimized computational intelligence model. The proposed model was developed and validated based on 47 laboratory data points and the Transit Search (TS) optimization algorithm. Using 80% of the experimental dataset, the optimized model was selected by determining the unknown coefficients of the network-based computational structure. The remaining 20% of the data was used to evaluate the accuracy of the model, and the best-performing structure was selected. Furthermore, the final neural network details were subjected to statistical analysis to extract a user-friendly formula, making it easier to apply in practice. The proposed ANN model and the proposed user-friendly formula were then compared with the AISC 341-16 and experimental results and demonstrated their efficacy in predicting the flexural behavior of composite shear walls. Overall, the proposed approach provides a more reliable and efficient framework for estimating the flexural behavior of composite shear walls.

Keywords: composite shear wall; reinforced concrete; flexural behavior; flexural capacity; optimization algorithm; soft computing; computational intelligence

Citation: Mirrashid, M.; Naderpour, H.; Kontoni, D.-P.N.; Jakubczyk-Gałczyńska, A.; Jankowski, R.; Nguyen, T.N. Optimized Computational Intelligence Model for Estimating the Flexural Behavior of Composite Shear Walls. *Buildings* **2023**, *13*, 2358. https://doi.org/10.3390/buildings13092358

Academic Editor: Bo-Tao Huang

Received: 28 August 2023
Revised: 7 September 2023
Accepted: 13 September 2023
Published: 16 September 2023

1. Introduction

A composite shear wall (CSW) comprises a matrix material surrounding walls with different elastic constants bonded to it [1]. There are three main classes of CSW, i.e., reinforced concrete (RC) panel infilled in composite frame, RC panel with embedded steel band bracing, and steel panel with or without covering the RC panel [2]. The resisting mechanism of these structural systems has been studied by Yamada and Osaka [2]. The resisting mechanism of a CSW combines two fundamentally opposite mechanisms [2]: the diagonal compression field of the infilled concrete and the diagonal tension field of the buckled steel panel. The diagonal compression field mechanism contributes to the CSW's initial stiffness and ultimate resistance by forming interconnected voids when the infilled concrete cracks diagonally under shear loading, allowing it to compress and resist shear forces. Achieving an optimal balance between these mechanisms involves designing the CSW with the right thickness of concrete and steel panel. The research by Yamada and Osaka [2] explores various factors affecting the CSW's resisting mechanism, such as shear span ratio, boundary conditions, and reinforcement details, concluding that CSWs offer versatility in meeting diverse seismic performance requirements.

The potential of CSW, compared to conventional shear wall systems, makes it a priority for choosing lateral bearing systems by structural designers, especially in tall buildings [3–5]. The CSW with concrete-filled steel tube (CFST) columns is one of the common lateral resistance systems. The steel plates in the CSW act as reinforcement once the concrete has hardened and transmitted the lateral loads via the floors and frame to the walls in tall buildings [6]. The column stiffness has a significant role in the overall behavior of CSW [7], and the presence of a steel plate deep beam in CSW can bring the deformation closer to that of the entire shear wall [8]. The hysteretic models for the CSW were proposed and evaluated for different loading configurations and cross-section shapes [9–11]. The effective stiffness of a CSW system consisting of a composite shear wall with double plates and filled with concrete has been numerically calculated, and the results were verified by a series of experimental tests [12]. Figure 1 represents a schematic view of three different composite shear walls (CSWs). Different section examples of a CSW can be found in the literature [9–13].

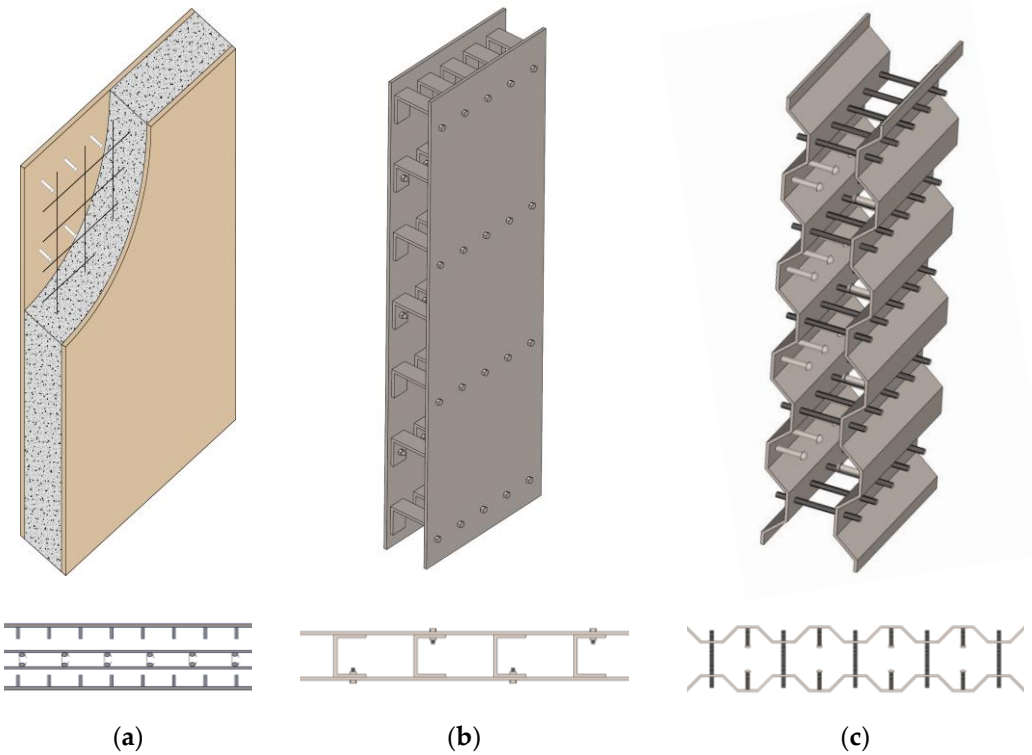

Figure 1. (**a**–**c**) Schematic view of three different composite shear walls (CSWs). (It is worth noting that in subfigure (**a**) for better 3D visualization, the authors have displayed only one mesh reinforcement grid that of the left 3D wall).

The effects of several parameters on the behavior of CSW have been evaluated in the literature. Previous studies indicated that the material properties of the bonded plates have high and low effects on the deflection and frequency of the RC shear walls strengthened with thin plates of carbon-fiber-reinforced polymer (CFRP), respectively [14]. The use of CFRP plates as externally bonded material can improve damaged RC shear walls [15], mainly due to the damping properties of the polymer. The CSW embedded with steel sections at the boundaries and middles of the RC walls enhances the ductility and energy dissipation than those with steel sections only at the boundaries [16]. The seismic behavior of CSW improves with an increase in steel areas at the end columns [16] and when considering the bending stiffness of the columns [17]. Furthermore, the ductility is influenced by the "bolt space" to "plate thickness" ratio [17] since it can prevent local buckling before yielding [18].

Composite plates greatly impact the behavioral characteristics of the CSW, such as displacement or frequency [19]. The seismic behavior of these structural elements depends on the geometrical factors of the shear wall and the frequencies of the earthquake [20]. Concrete thickness is one of the parameters that when increased reduces shear steel plate buckling [21] and enhances the ultimate strength of the CSW [22]. Moreover, reducing the distance between the connectors may cause more energy dissipation [21]. Dey and Bhowmick proposed two equations to estimate the connector spacing and thickness of reinforced concrete panels in CSW [23]. They also introduced a formulation to predict the period of the CSW system. Damage states and repairing techniques of CSW were also studied by researchers [24]. The seismic performance of embedded CSW containing high-strength concrete can improve the deformation, load, and energy dissipation capacities [25]. Seo et al. [26] defined a shear force–shear strain model considering the in-plane shear behavior of SCW. In another study, displacement–force equations were obtained [27] for CSW systems. Previous studies indicated that at the beginning of loading in an infill composite wall (CSW), the interaction between concrete and steel increases until the shear yield of the steel plate [28]. The encased steel plates, e.g., horizontal and vertical corrugated, in CSW systems represent different shear-sharing ratios [29]. Furthermore, the critical buckling stress and flexibility in CSW can be limited considering tie spacing, plate slenderness, and flexural rigidity of the steel plates [30]. Finite elements models are one of the most important techniques that have been discussed in the analytical studies of CSW. Some researchers developed these models to investigate the structural behavior of the CSW [31–35].

In recent years, numerous studies have been conducted to investigate the performance of various structures derived from the different classes of CSW; some of which have led to the introduction of specific models of such systems. For example, shear walls infilled with concrete having bundled channels [36], CSW with concrete-filled steel tube (CFST) columns connected to beams only [37], precast slender CSW with CFST boundary elements [38], multi-partition CSW [39], RC wall web having square CFST columns as boundary elements incorporating CFRP-confined concrete core [40], encased steel plate-reinforced gangue CSW [41], double-skin profiled wall [42], CSW infilled with concrete having dual steel plates with vertical stiffening steel plates [43], CSW with high-strength concrete and steel rebars with consideration of concrete-encased CFST columns as boundary elements [44], and CSW with FRP-confined concrete cores [45] or enhanced C-channels [46] can be mentioned.

The shear strength is one of the key parameters that has been evaluated in the literature for CSW. To avoid shear failure in these systems, ensure reliable stiffness, and control the inter-story drifts, researchers recommended designing the RC walls for the shear force of the capable bending moment [47]. In some cases, mathematical formulations and new methods were introduced to predict the shear capacity of such lateral-resistant systems [48–51]. The value of this parameter can be decreased with increasing initial axial tension or in the presence of out-of-plane eccentricity in CSW [52]. Mo et al. reviewed the design techniques and seismic studies for CSW systems [53].

2. Research Significance

In recent years, there have been numerous studies examining the performance of composite shear wall (CSW) systems. Many researchers have utilized experimental results to develop hysteretic and finite element behavioral models. Among the critical aspects of structural elements, determining their ultimate strengths is of utmost importance. Accurate estimation of these values can enhance our understanding of structural behavior and aid in the selection of retrofit methods and strengthening of elements. Despite the significant research on estimating the shear strength of CSW systems, there is limited information available on their flexural capacity. This gap can be attributed to the scarcity of adequate laboratory data required for statistical modeling. Therefore, this article proposes a novel method that employs computational intelligence techniques, such as neural networks and meta-heuristic optimization algorithms, to perform and validate flexural capacity prediction

models of CSW systems using laboratory results. A continuous statistical sequence is created using the resulting artificial neural network (ANN) system to formulate a user-friendly prediction formula. The proposed ANN model and the proposed user-friendly formula are compared with the AISC 341-16 [54] results and existing experimental tests, and the results are thoroughly discussed, providing valuable insights into the behavior of CSW systems.

3. Database

In order to determine the appropriate model for estimating the flexural capacity of composite shear walls based on the approaches used in this article, it is first necessary to collect a set of laboratory data. For this purpose, experimental results related to CSW tests (47 tests) have been gathered from the literature [55]. For each of the data, 11 variables including the wall height, the section length, the thickness of the wall web, the length of the boundary element (BE), the thickness of the boundary element, the steel plate thickness in the boundary element, the steel faceplate thickness, the yield strength of steel faceplate, the yield strength of steel in boundary element, the concrete strength, and also the axial stress (axial load divided to the wall section area) were considered as input while the flexural capacity was selected as the target. The statistical details of the parameters and their distribution are given in Table 1 and Figure 2, respectively. Distribution plots of the input variables against the targets are also presented in Figure 3.

In order to use the above data, their values were normalized into the range of 0 and 1 by Equation (1), and then, 37 data points were randomly chosen to be used in the process of determining the optimal architecture of the models. In this equation, $X_{i,n}$, X_{min}, and X_{max} are the normal, minimum, and maximum values of the X_i, respectively. The remaining 10 data points were used to evaluate the proposed model's ability to predict the output.

$$X_{i,n} = \frac{X_i - X_{min}}{X_{max} - X_{min}} \quad (1)$$

Table 1. Statistical details of the database.

Variable	Unit	Name in This Research	Minimum	Maximum	Mean	St. Dev.	Median
Wall height	mm	X_1	750.00	3850.00	2379.34	658.06	1200
Section length	mm	X_2	750.00	1284.00	1055.41	175.93	2016
Thickness of the wall web	mm	X_3	90.00	214.00	143.24	42.82	2350
Length of the boundary element	mm	X_4	0.00	280.00	165.16	71.13	1020
Thickness of the boundary element	mm	X_5	100.00	219.10	152.50	42.05	140
Steel plate thickness in boundary element	mm	X_6	2.94	10.00	5.01	2.12	150
Steel faceplate thickness	mm	X_7	1.83	10.00	4.78	2.27	140
Yield strength of steel faceplate	MPa	X_8	245.00	443.00	335.49	56.12	4.71
Yield strength of steel in boundary element	MPa	X_9	245.00	443.00	331.01	55.37	4.08
Concrete strength	MPa	X_{10}	25.30	92.60	49.18	21.42	322
Axial stress	MPa	X_{11}	0.00	30.04	12.59	9.67	306
Flexural capacity	kN.m	Y	858.00	6929.00	2868.19	1942.09	41.3

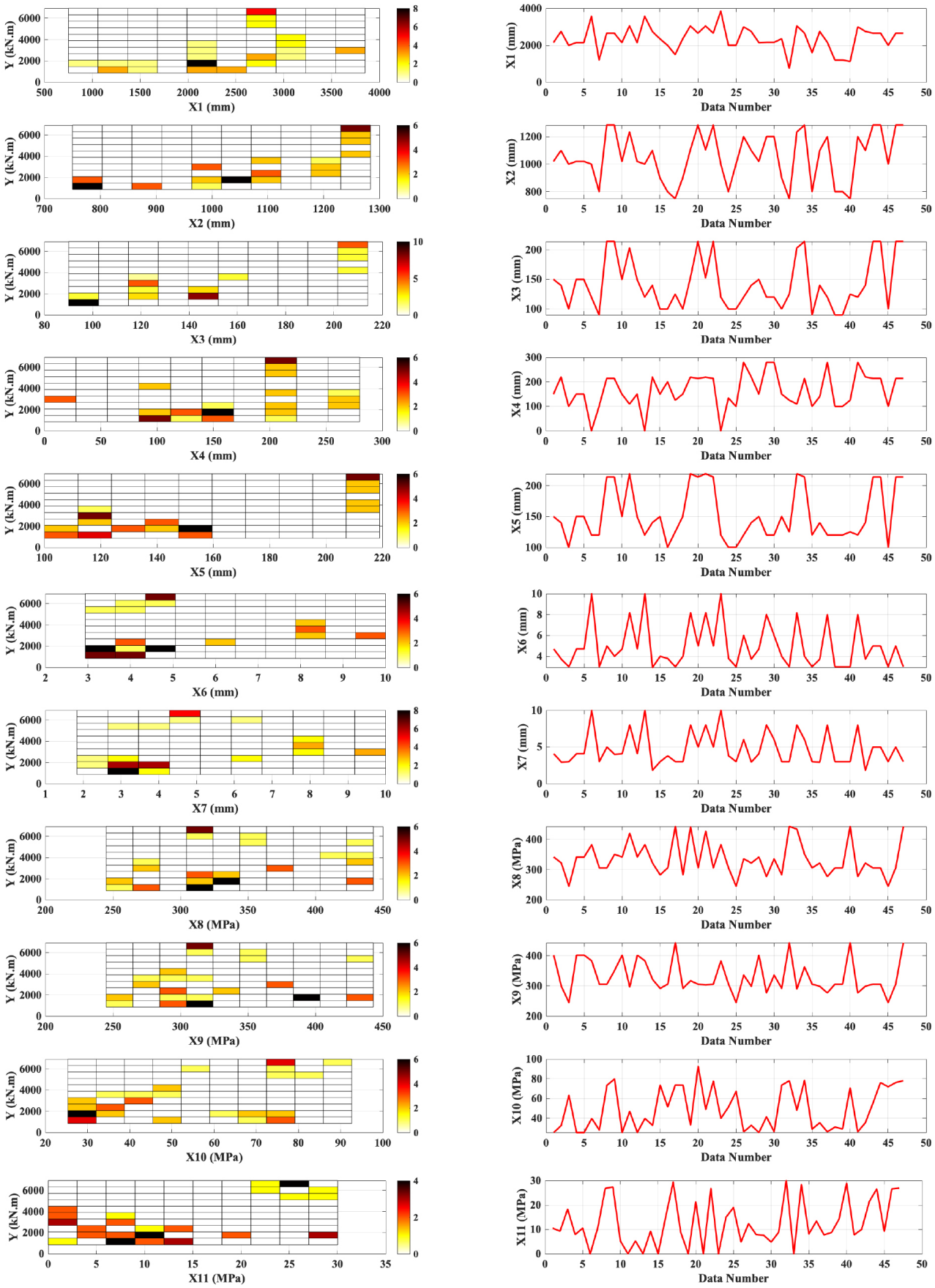

Figure 2. Distribution of the 47 experimental datasets.

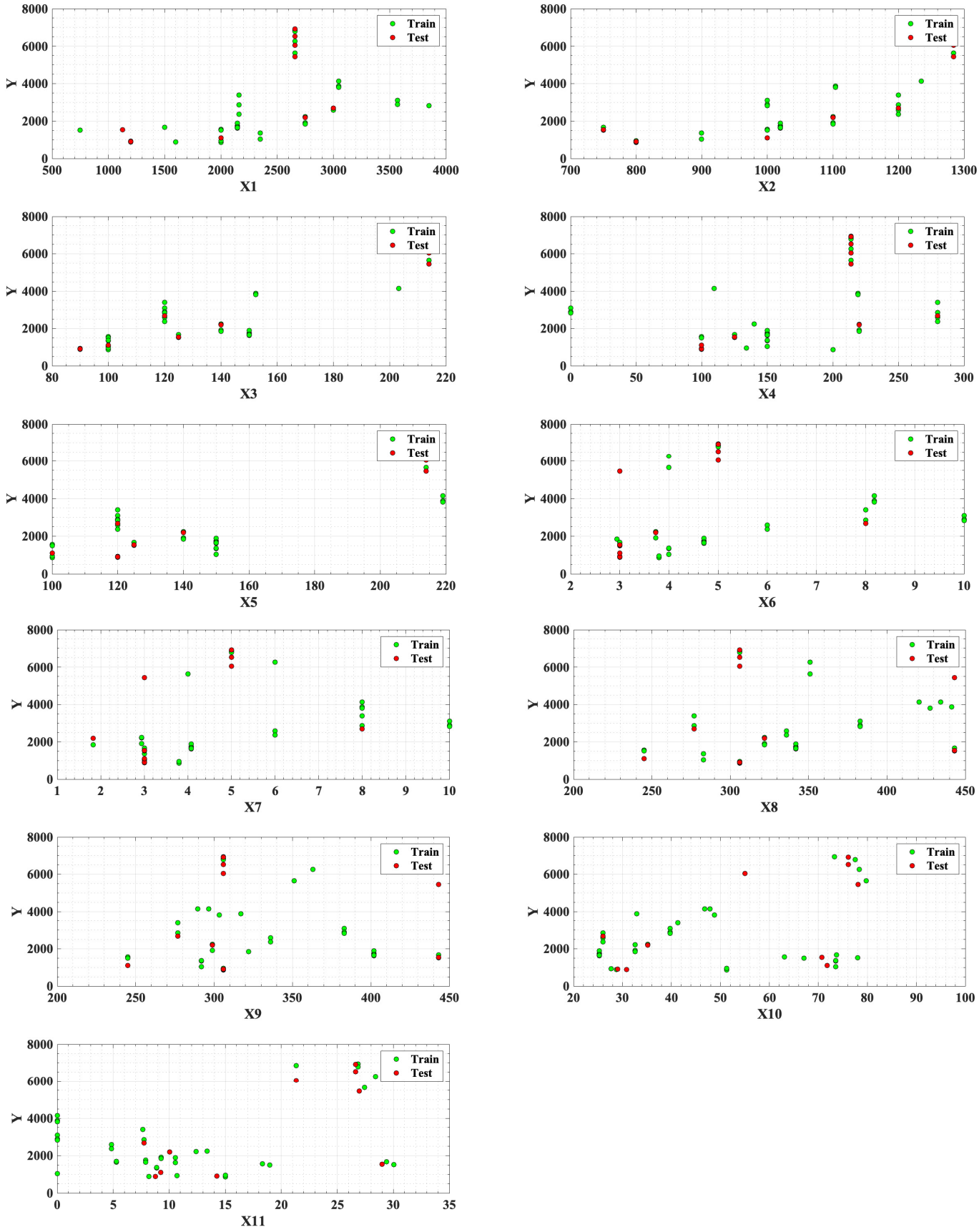

Figure 3. Distribution plots of the input variables vs. the target.

4. The Proposed Approach

Nowadays, the use of soft computing (SC) methods in solving various engineering problems is widespread [56–59]. The reason for this can be attributed to flexibility, high accuracy, application in nonlinear and complex models, and the ability to combine different methods in order to take advantage of them together. In this article, the authors have used artificial neural network (ANN) models [60] to provide a computational framework to predict flexural capacity. The Transit Search (TS) optimization algorithm [61] was considered to determine the unknown parameters of the neural networks. The TS algorithm is an innovative optimization technique inspired by the astrophysical exoplanet exploration method known as "transit". Transit has proven to be a highly effective approach for detecting exoplanets, with more than 3800 planets discovered using this method from space telescope databases. Detecting these planets is challenging due to their minute size within the vast cosmos. Capitalizing on the efficiency of the transit method in astrophysics, the TS optimization algorithm was introduced in the literature for optimization purposes. In the transit algorithm, changes in luminosity are meticulously examined by monitoring the light received from stars. By using the neural network with the best performance, a step-by-step approach has been performed to extract mathematical and user-friendly relationships from the selected neural network. This increases the efficiency of the proposed model and provides the ability to use it in a simple form for researchers and engineers. Details of the model and its determination process are provided in the following sections.

4.1. Optimization of the Neural Networks

The operation of artificial neural networks (ANNs) is based on the fundamental principle of human neural networks. Information is directed to the network's cells, where it is processed, remembered, and utilized in the future. Just like in the human brain, artificial neural systems operate in a similar manner. They receive, process, and store information and can even correct themselves. Similar to the interconnected cells in a human neural network, ANNs can communicate with each other, forming a multilayer network that enhances the computational capabilities of the algorithm.

To develop an effective ANN model, a substantial database is required. These data are used to determine the unknown coefficients of the computational model and evaluate its performance. A larger amount of available data typically leads to suitable accuracy in the model. However, in this research, the database contains only 47 data points, which may not be sufficient to achieve an efficient ANN model. Therefore, an optimization algorithm has been applied instead of a common learning process to determine the coefficients of the ANNs, as shown in Figure 4.

In each iteration of the algorithm, the initial values of the weights and biases of the network are replaced with the best values obtained so far. Subsequently, the input vector of each of the 37 data points is applied to the network, and the corresponding output is calculated (as shown in Figure 5). By comparing the network outputs with the laboratory values, the network error is determined. The objective function of the optimization algorithm in this method is to minimize the root mean squared error (RMSE).

The proposed method in this article employs a neural network with one middle layer. Initially, the number of neurons in this layer is set to 1, and the optimization algorithm is applied with 400 iterations to obtain the optimal values for the weights and biases of the network. Then, the number of neurons is incrementally increased by one, and the algorithm is applied again to determine the network coefficients. This process is repeated for a range of 1 to 30 neurons, allowing for a thorough exploration of different network configurations.

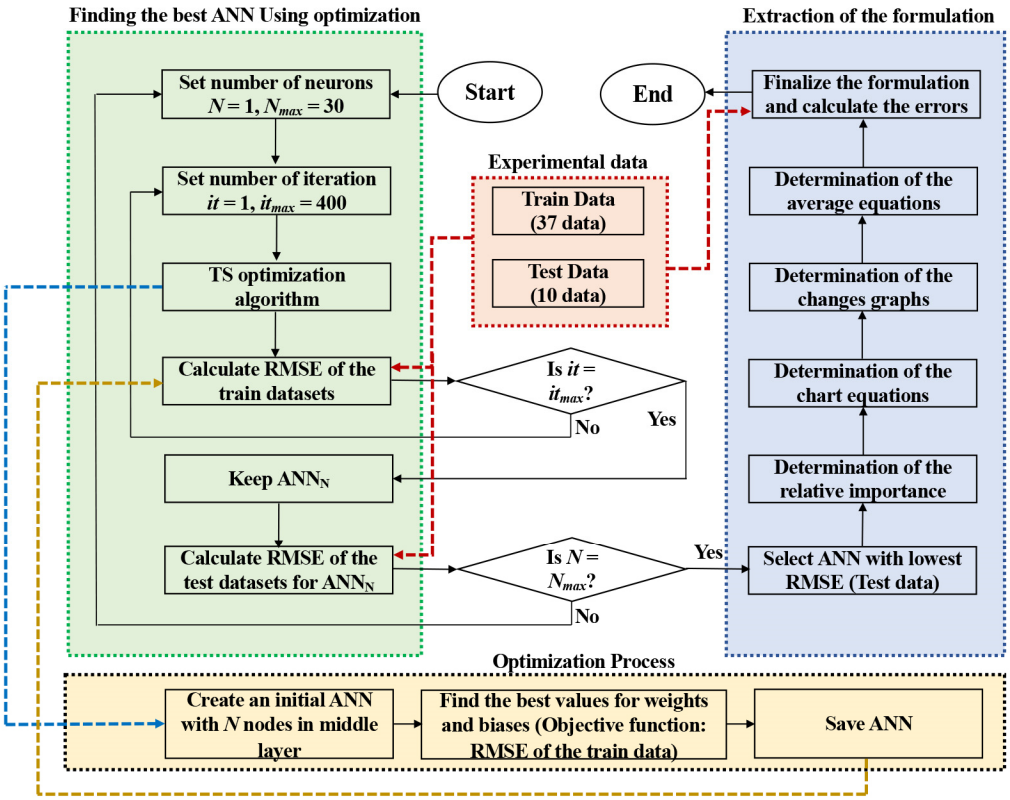

Figure 4. Optimization process to determine the best ANN.

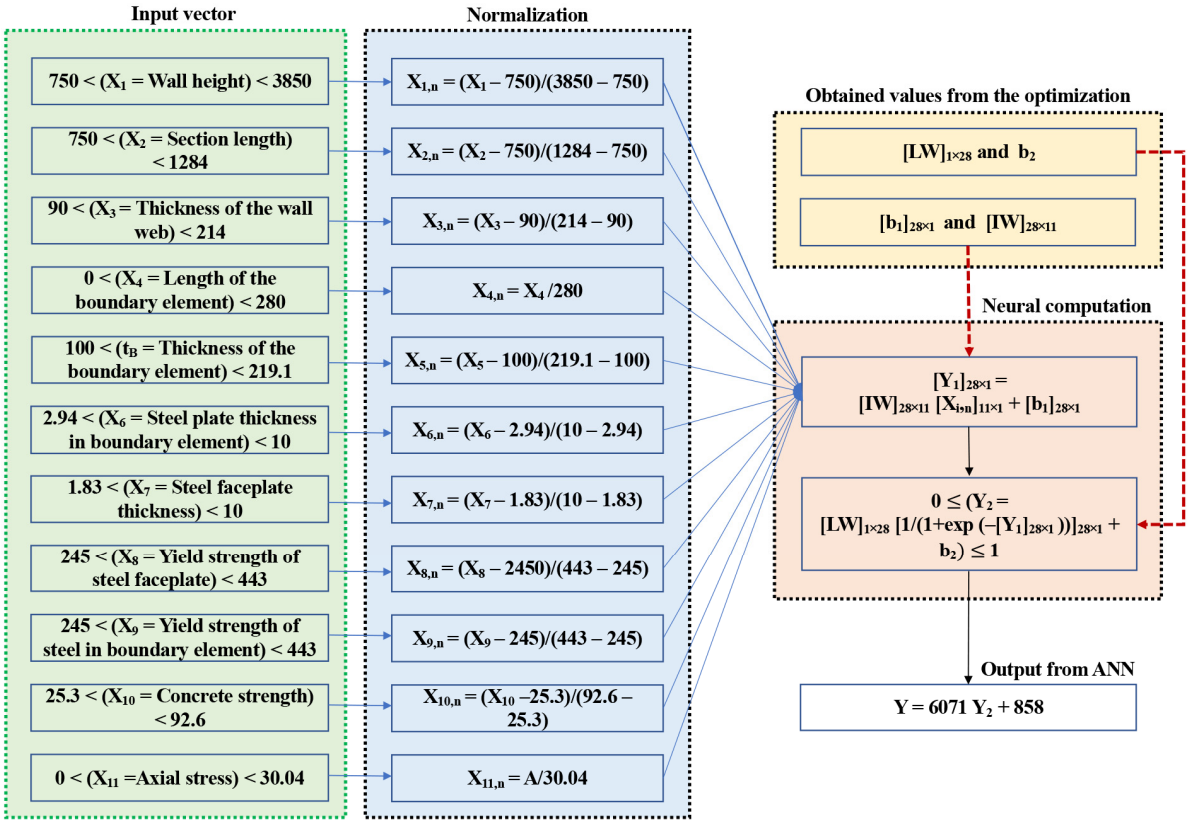

Figure 5. Architecture of the ANN.

4.2. Model Selection

As mentioned earlier, a total of 30 optimized neural networks were obtained to determine the target parameter, which is the flexural capacity of CSW members in this article. The architectural difference among these networks lies in the number of neurons in the middle layer, ranging from 1 to 30. For the identification of each of these networks, a 400-iteration optimization algorithm was employed, utilizing 37 datasets to determine the associated costs. The progression of the objective function (RMSE) values for each iteration is visually presented in Figure 6. After thorough analysis, it was observed that the network with the most favorable cost performance boasted 28 nodes within its middle layer.

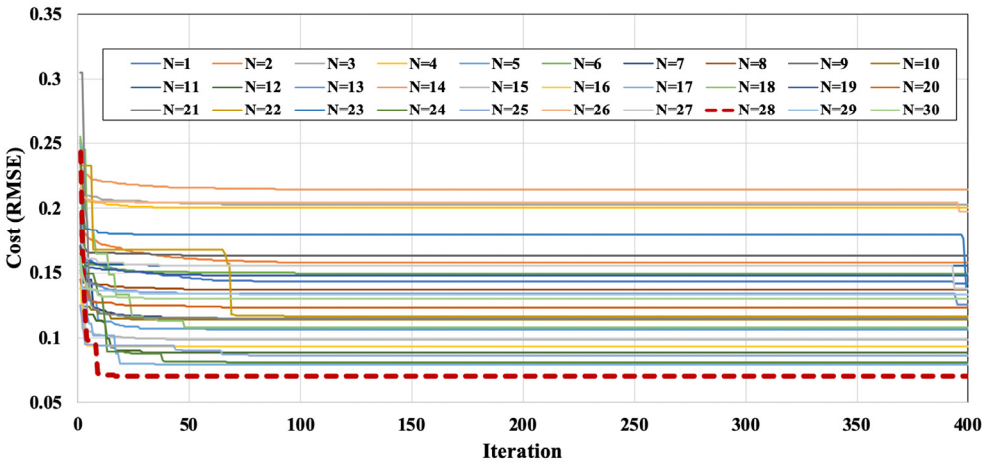

Figure 6. Cost values during optimization.

To further investigate the performance of each of the 30 neural network models, both training (37 data) and test (10 data) datasets were applied to the networks, and RMSE values were obtained for each. The results are illustrated in Figure 7. It is evident from Figure 7 that the network with 28 neurons in the middle layer has the lowest error values for both datasets. As a result, this network is selected as the final neural network model in this article, taking into consideration its superior performance in predicting the flexural capacity of CSW systems.

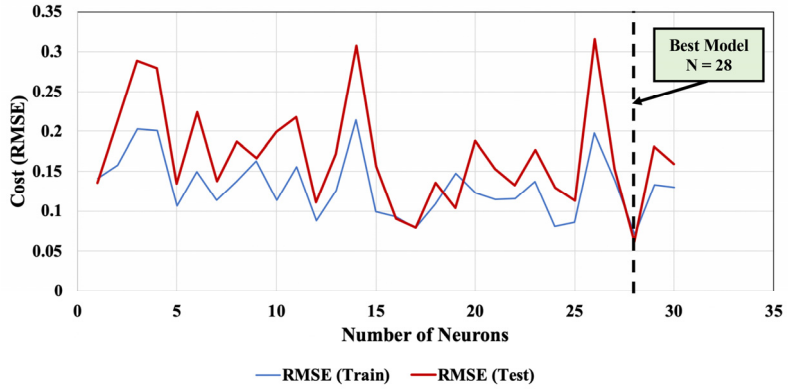

Figure 7. The results for the ANN models with different numbers of neurons.

In the proposed model for estimating the flexural capacity of RC composite shear walls based on the proposed ANN directly, it is first necessary to calculate the normalized values of each input variable according to Equation (1) or Figure 5. Then, the final output of the middle layer (Y_1) will be determined using Equation (2). By applying the layer weight and corresponding bias values to the corresponding node, the normalized output of the ANN is obtained by Equation (3). Given that this value is normalized (between 0 and 1),

it should be converted to its real value with consideration of Equation (4). The values of input weight (IW), layer weight (LW), and bias (b_1 and b_2) for the proposed ANN are given in Tables 2 and 3.

$$[Y_1]_{28\times1} = [IW]_{28\times11}\,[X_{i,n}]_{11\times1} + [b_1]_{28\times1} \quad (2)$$

$$0 \le (Y_2 = [LW]_{1\times28}\,[1/(1 + \exp(-[Y_1]_{28\times1}))]_{28\times1} + b_2) \le 1 \quad (3)$$

$$Y_{ANN}\ (\text{kN.m}) = 6071\ Y_2 + 858 \quad (4)$$

Table 2. Input weights for the best ANN.

Neuron	Input 1	Input 2	Input 3	Input 4	Input 5	Input 6	Input 7	Input 8	Input 9	Input 10	Input 11
N1	−0.011503	−0.004022	−0.002823	−0.000002	0.000000	0.001313	−0.007224	−0.018706	0.001310	−0.001246	−0.001350
N2	−0.003010	0.000005	0.002786	−0.000007	−0.001349	0.013977	0.000000	−0.002840	0.000001	−0.006054	−0.001337
N3	0.000966	0.003575	−0.003528	0.000143	0.000007	0.003397	−0.000949	−0.002801	0.000005	−0.002819	−0.004304
N4	0.000000	−0.000019	−0.000019	−0.002874	0.000002	0.000215	0.000621	0.001310	−0.001844	0.000003	−0.004217
N5	0.006638	−0.004013	0.000002	0.000000	−0.000002	−0.001310	0.000000	0.000002	−0.001262	0.001310	−0.001307
N6	0.000923	0.001884	−0.000049	0.002092	0.000000	−0.000927	−0.010491	0.003001	0.001871	0.004747	0.000000
N7	0.001925	−0.004841	0.000002	0.001310	0.000000	0.002856	0.000042	0.000000	0.006810	0.002394	0.004729
N8	0.000002	0.001655	−0.000318	−0.001310	0.002144	−0.000018	0.000041	−0.001530	0.001662	−0.001723	0.000000
N9	−0.000983	−0.000197	−0.001304	−0.001331	0.004399	0.001291	−0.002109	0.002820	0.003538	0.000162	−0.001579
N10	−0.000019	0.000217	−0.000090	0.000007	−0.001309	1.955827	−0.001317	0.000000	0.010353	−0.000019	−0.008409
N11	−0.008876	−0.006932	−0.012903	0.000000	−0.000006	0.001730	0.000000	0.001313	0.000019	−0.001313	−0.005812
N12	−0.001287	−0.000219	−0.000018	−0.000001	−0.000002	−0.000057	−0.001692	−0.001350	−0.000004	0.000002	−0.000004
N13	0.000000	−0.009142	−0.000192	0.000010	−0.001310	0.001310	0.000000	0.000000	0.000001	−0.008685	−0.004695
N14	0.000000	−1.305027	−0.000010	−0.003954	0.001310	0.002722	−0.000010	0.005397	−0.000004	−0.000199	−0.000303
N15	0.000000	0.000219	0.009769	−0.000267	0.013826	0.000002	−0.001490	−0.000042	0.001307	−0.000002	−0.001310
N16	0.000947	−0.002846	−0.001979	−0.001330	0.000000	−0.006541	−0.006685	−0.002095	0.000218	0.000218	0.004712
N17	−0.003684	−0.000005	0.000000	−0.000104	0.000000	0.008035	0.001310	0.008684	0.000018	−0.001307	−0.001655
N18	−0.000218	0.004706	−0.000002	0.000000	0.001828	0.000000	0.000000	0.001929	−0.000960	−0.000226	1.931129
N19	0.002160	0.001310	0.000219	−0.006635	0.002873	−0.001222	0.009734	−0.000691	−0.002075	0.000004	−0.001307
N20	−0.000966	−0.000018	−0.001310	0.001327	−0.001313	−0.000049	0.000234	0.000003	−0.000019	−0.002786	0.001000
N21	0.000000	0.001307	−0.000961	0.000000	−0.000003	0.000002	−0.000019	−0.000019	0.000003	0.006654	0.000962
N22	−0.000752	0.006077	−0.001316	0.000000	−0.001313	0.001307	0.000000	0.001389	0.001310	0.002226	0.001248
N23	−1.970320	−0.006568	−0.001291	−0.005663	−1.814332	0.000002	−0.864744	0.000002	−0.000002	0.001310	−0.001318
N24	0.002908	0.006066	0.000000	−0.002092	−0.001304	−0.004567	−0.000166	−0.004562	0.002824	0.000000	0.003524
N25	0.000097	−0.000923	−0.001290	−0.000064	0.005243	−0.000004	0.000000	−0.000984	−0.001854	−0.000009	0.000219
N26	0.001313	0.008380	−0.001642	0.002823	0.002791	−0.002075	0.000004	0.001310	0.001200	0.000004	−0.000007
N27	0.000218	0.000019	0.000004	−0.000255	0.001335	−0.001310	−0.001403	−0.000234	−0.000040	0.000006	0.000000
N28	−0.000028	−0.000019	0.000019	0.000019	−0.000028	0.006925	−0.000745	0.001313	−0.002839	0.000000	0.001295

Table 3. Biases and the layer weights for the best ANN.

Neuron	Bias 1	LW	Bias 2
N1	0.000049	0.463061	0.006269
N2	−0.002855	−0.000004	-
N3	0.001655	0.018138	-
N4	0.004712	0.000000	-
N5	−0.000166	−0.000002	-
N6	−0.001330	0.145684	-
N7	0.000019	0.008551	-
N8	0.000959	−0.000219	-
N9	0.000018	0.002786	-
N10	0.001301	−0.000065	-
N11	−0.001646	−0.000307	-
N12	0.000002	−0.000215	-
N13	0.002143	0.000000	-
N14	−0.001266	−0.815577	-
N15	−0.004587	−0.000090	-
N16	−0.004343	−0.002167	-
N17	−0.003749	−0.000019	-
N18	0.000019	0.974563	-

Table 3. *Cont.*

Neuron	Bias 1	LW	Bias 2
N19	0.000000	0.001357	-
N20	−0.002839	−0.000019	-
N21	−0.003281	−0.000019	-
N22	−0.001925	0.000000	-
N23	0.001316	−1.290456	-
N24	−0.000009	0.022915	-
N25	0.001086	0.001310	-
N26	−0.000060	0.000253	-
N27	0.000000	−0.001530	-
N28	0.002856	0.001310	-

4.3. Extraction of a User-Friendly Equation from the Proposed ANN

In this section, the final neural network model, as defined in the previous section, is utilized. The primary objective here is to extract mathematical relationships that can determine the flexural capacity of CSW members from the proposed ANN structure. To achieve this, the first step is to identify the input variable that has the most significant impact on the output. This is performed through sensitivity analysis, which involves investigating the effect of changes in each input on the output. The results of the sensitivity analysis are presented in Figure 8, illustrating the findings obtained. To perform this analysis for variable X_1, first, the values of parameters X_2 to X_{11} were considered equal to their average value (see Table 1). Then, the network output was obtained for different values of X_1. The above process has been carried out for other input variables as well. According to Figure 8, it is clear that changes in the input parameters directly impact the output for all input variables. Therefore, the authors used the relationship introduced by Milne [62] to determine the most effective input parameter. This relationship [62], which is shown by Equation (5), calculated the relative importance of each variable on the output based on the weight values of the neural network.

$$Q_{ik} = \frac{\sum_{j=1}^{n_{hidden}} \frac{W_{ji}}{\sum_{l=1}^{n_{input}} |W_{jl}|} W_{oj}}{\sum_{k=1}^{n_{input}} \left(\sum_{j=1}^{n_{hidden}} \left| \frac{W_{jk}}{\sum_{l=1}^{n_{input}} |W_{jl}|} W_{oj} \right| \right)} \quad (5)$$

In this equation, Q_{ik}, W, j, i, k, n_{hidden}, W_{oj}, and n_{input} are the percentage of the impact of each parameter, the weight, layer node number in the middle layer, input node number, output node number, number of nodes in the middle layer, and the number of inputs, the connection weight between the middle layer nodes and the output node, respectively.

Using Equation (5), the relative importance percentages of each input variable are calculated, the values of which can be seen in Figure 8. Accordingly, the most effective parameter is the X_2, with 13.78% impact on the output. This variable, which represents the section length of the RC composite shear wall, is known as the chart parameter in this article.

The relative importance parameter is an input variable that has the most significant impact on the output, which in this case is the section length of the RC composite shear wall. This parameter is derived from a sensitivity analysis, which involves systematically investigating how changes in each input variable affect the output of our neural network model. By performing regression in the results of sensitivity analysis for this variable, Equation (6) was determined to calculate the Y_{chart}.

$$Y_{chart} = 2.827\ X_2 - 247.19 \quad (6)$$

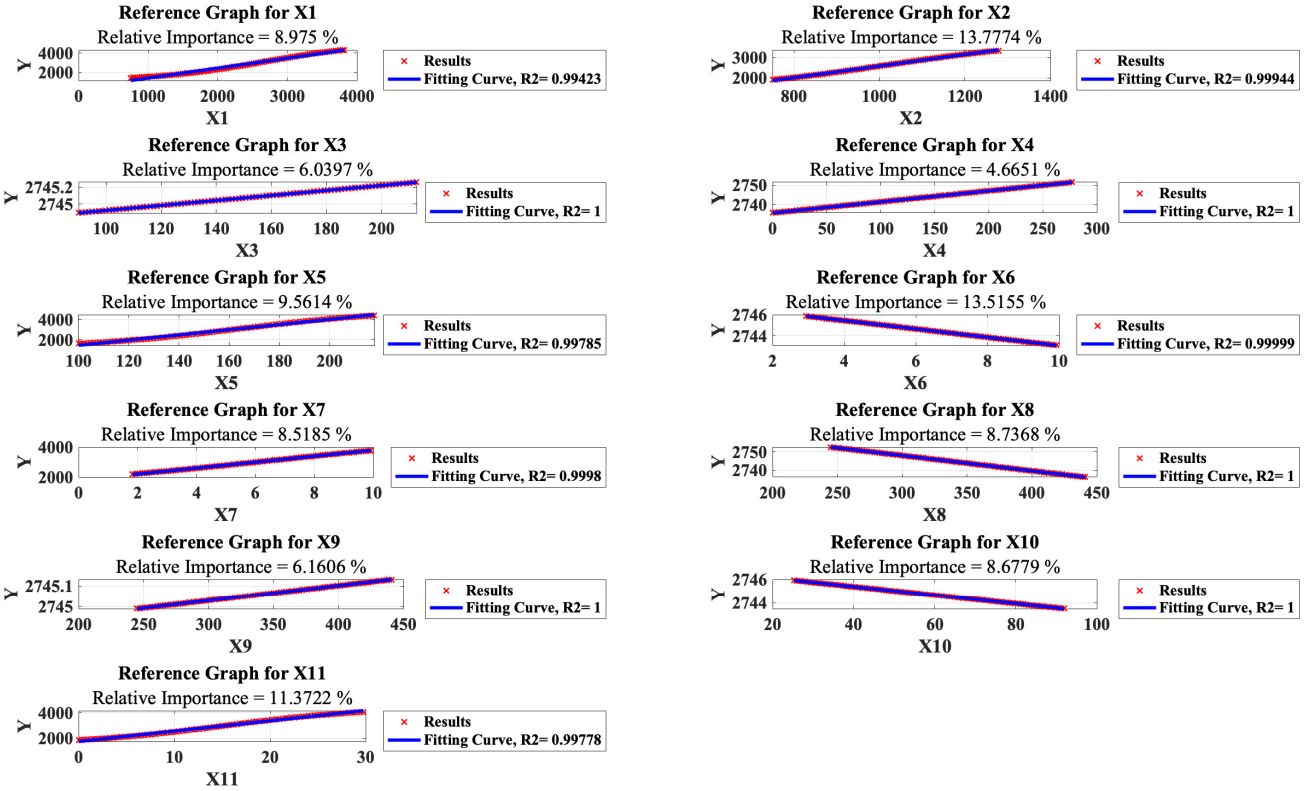

Figure 8. Reference graphs for the input variables.

After determining the chart equation, a new database was created to determine the outputs using the proposed ANN. For this purpose, 50 datasets were generated each time the network was implemented. In the first step, all input values were set to their averages (as displayed in Table 1), except for the first input, which was varied from its minimum to maximum values in 50 steps. This process was repeated for 10 different sets of 50 databases, with the second variable being changed 10 times and one value from each set being applied to each of the 10 collections. After completing the 10 sets of 50 databases for the first variable, the network output for each database was determined. The results are presented in Figure 9, depicting the changes in the entire input variables. The parameter C(X) in Figure 9 represents the correction for input variable X, which indicates the ratio between the ANN output and the corresponding value obtained from the network for the dataset with average input values.

The average of the graph of the change for each input is shown in Figure 10. The relationship for each curve is shown in Equations (7)–(16):

$$C(X_1) = 0.856\ X_1 + 0.173 \tag{7}$$

$$C(X_3) = 8.75 \times 10^{-5}\ X_3 + 1 \tag{8}$$

$$C(X_4) = 0.0033\ X_4 + 0.997 \tag{9}$$

$$C(X_5) = 1.39\ X_5 - 0.371 \tag{10}$$

$$C(X_6) = -7.26 \times 10^{-4}\ X_6 + 1 \tag{11}$$

$$C(X_7) = 0.331\ X_7 + 0.674 \tag{12}$$

$$C(X_8) = -0.01\ X_8 + 1.01 \tag{13}$$

$$C(X_9) = 1.1 \times 10^{-4}\, X_9 + 1 \tag{14}$$

$$C(X_{10}) = -6.1 \times 10^{-4}\, X_{10} + 1 \tag{15}$$

$$C(X_{11}) = 0.373\, X_{11} + 0.639 \tag{16}$$

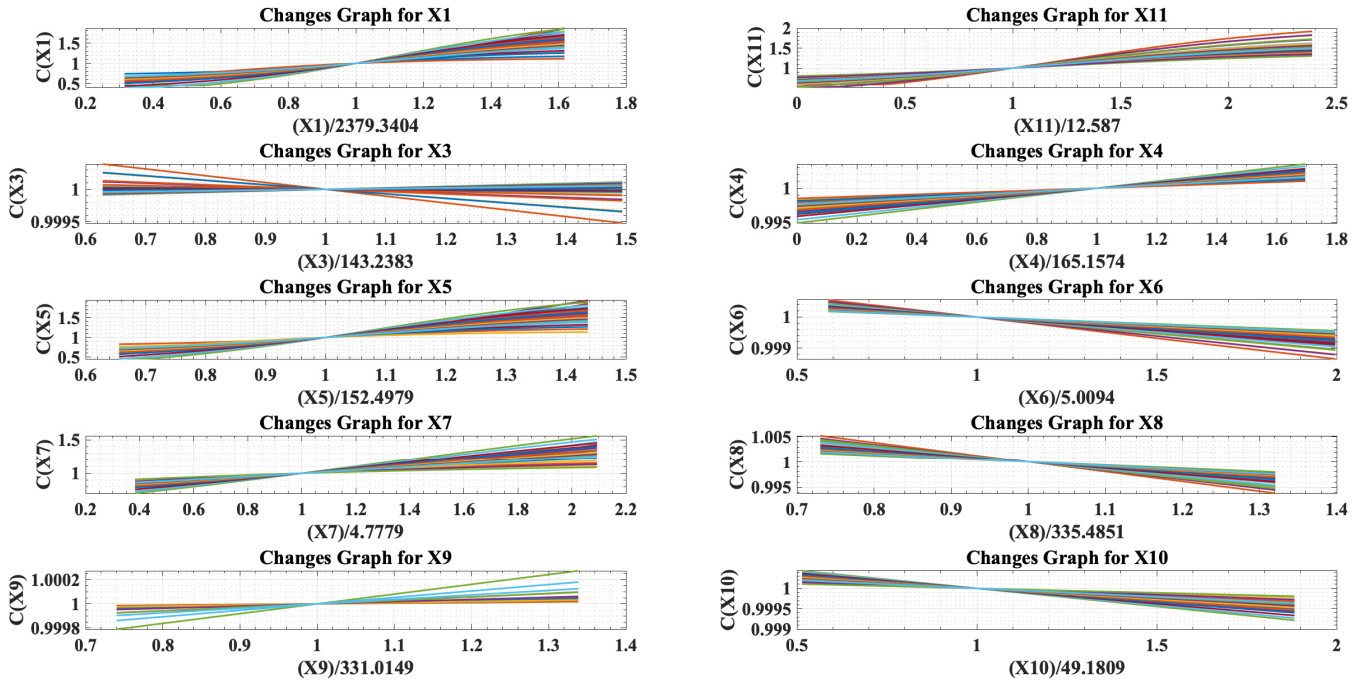

Figure 9. Changes graphs for the input variables.

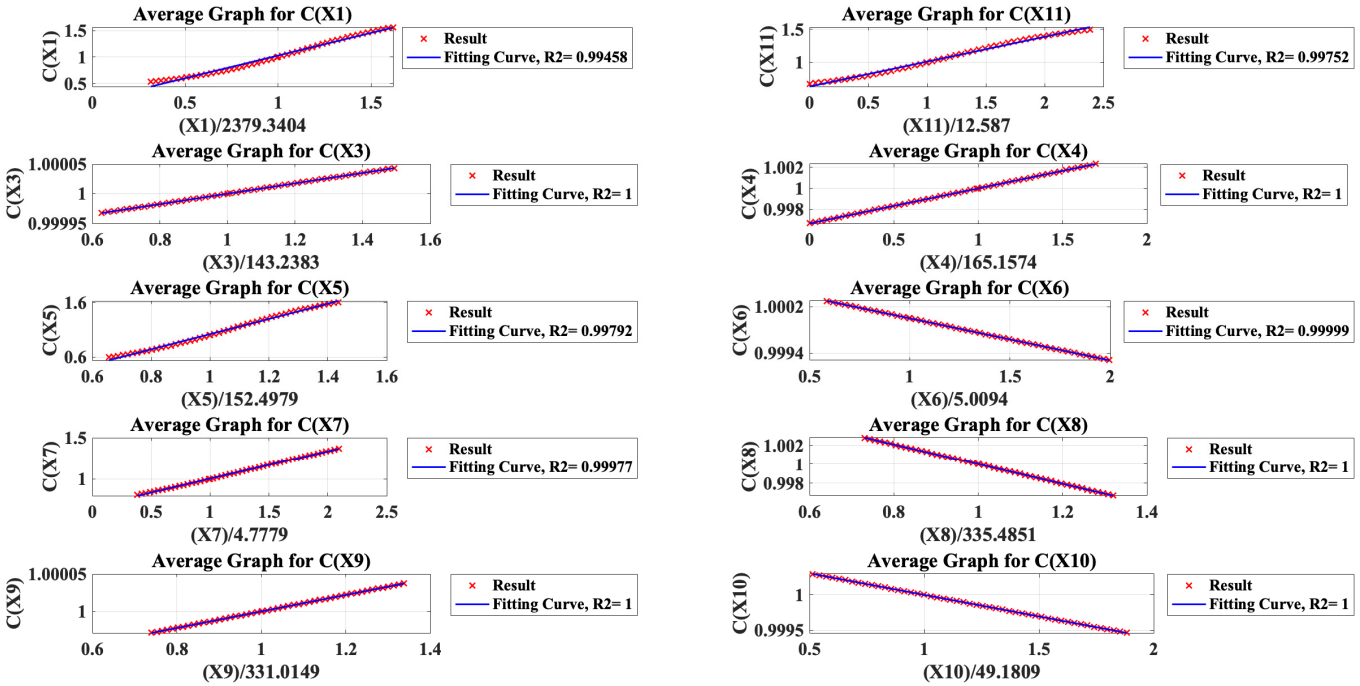

Figure 10. Average graphs for the input variables.

Once the relationships of the chart equation (Equation (6)) and the average curves (Equations (7)–(16)) are determined, the flexural capacity of CSW members, Y, can be simply calculated (in kN.m) using the user-friendly Equation (17):

$$858 \leq Y\,(\text{kN.m}) = Y_{chart}\, C(X_1)\, C(X_3)\, C(X_4)\, C(X_5)\, C(X_6)\, C(X_7)\, C(X_8)\, C(X_9)\, C(X_{10})\, C(X_{11}) \leq 6929 \quad (17)$$

5. Comparison Study

In this section, the results obtained for the proposed neural network model and the formula derived from it (Equation (17)) are compared with the AISC 341-16 [54]. In order to determine the flexural capacity of the CSW members, 47 laboratory data points used in this article were considered. The input vector of each dataset, which includes 11 variables, was applied to the three computational models mentioned above to calculate the flexural capacity. Subsequently, the results were compared with the values reported by the laboratory. The findings indicate that both models proposed in this article exhibit an acceptable accuracy compared to the composite flexural strength provided by the AISC 341-16 seismic provisions, which underestimated the experimental test results (as depicted in Figure 11).

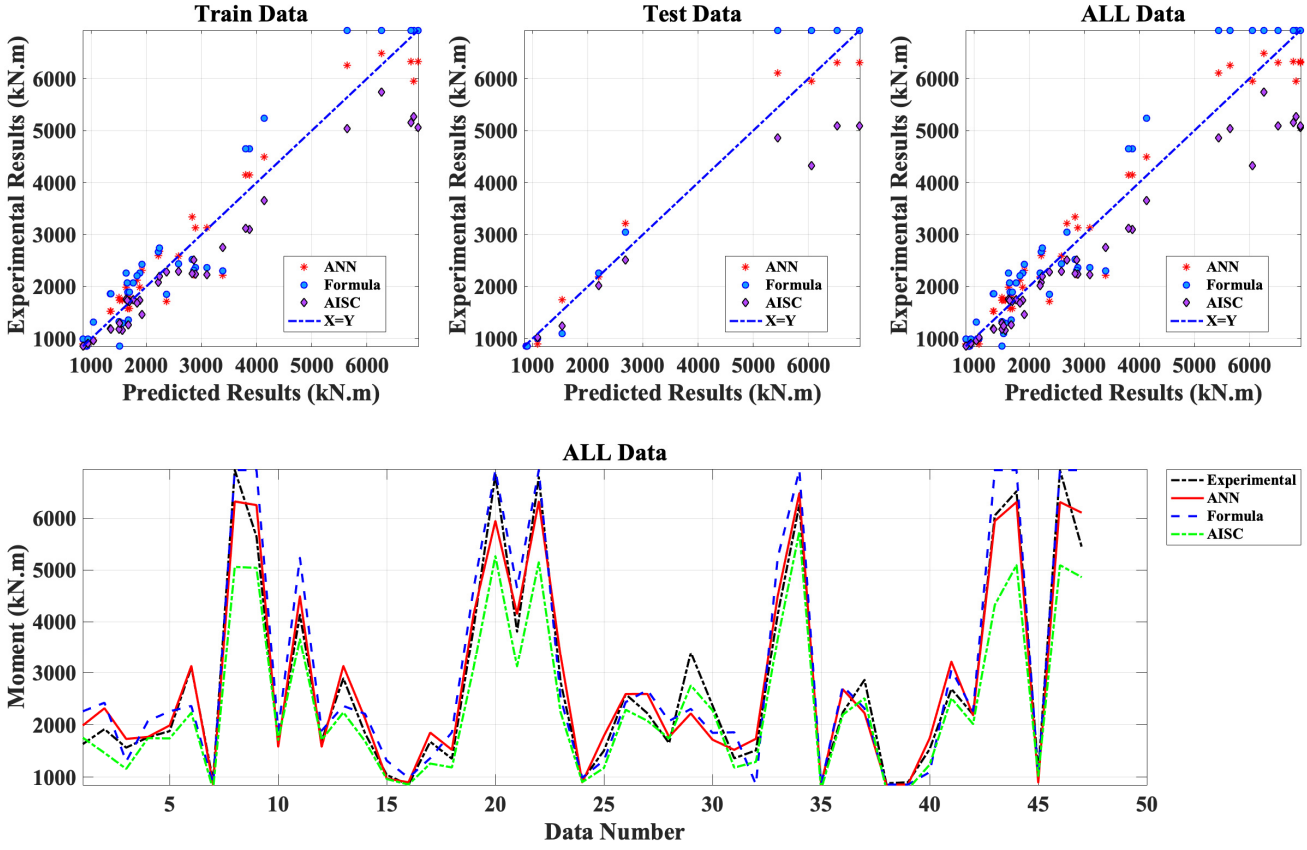

Figure 11. Comparison results.

In order to comprehensively assess the performance of each method, the root mean squared error (RMSE) and mean absolute error (MAE) were evaluated separately for the train and test datasets. The results are presented in Figure 12 (as radar graphs) and Table 4. For the proposed artificial neural network (ANN), the RMSE and MAE for the test data were found to be 350.83 and 260.48, respectively. In contrast, the RMSE and MAE values for the proposed formula (Equation (17)), which was extracted from the neural network structure using a step-by-step statistical approach, were 590.42 and 380.69, respectively. Furthermore, the error values for the AISC 341-16 seismic provisions, which yielded higher values compared to both proposed models, were also calculated. Based on the obtained

error parameters, it can be concluded that the two models proposed in this article exhibit good accuracy in estimating the flexural capacity of CSW members.

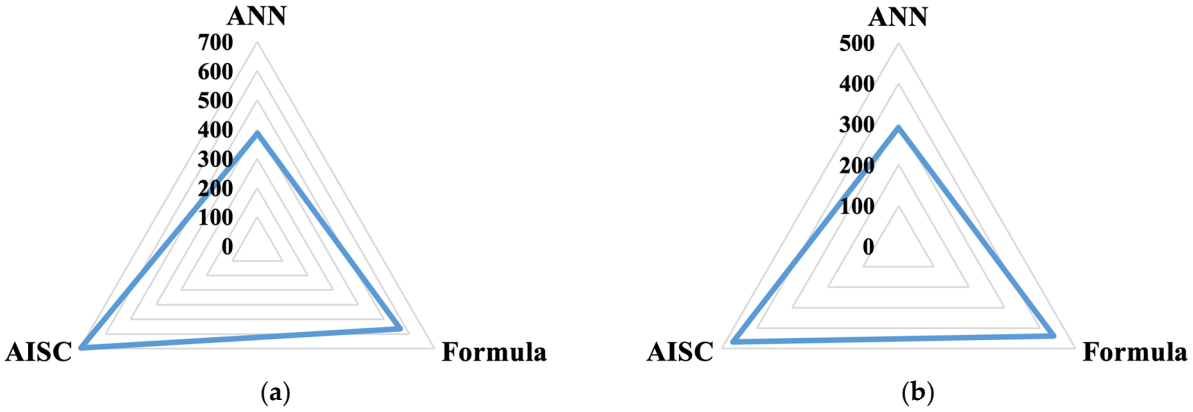

Figure 12. Statistical values for the two proposed models (ANN and Formula) and the AISC 341-16 results: (**a**) RMSE and (**b**) MAE.

Table 4. A summary of the comparison results.

Parameter	The Proposed ANN			The Proposed Formula			AISC		
	Train	Test	All	Train	Test	All	Train	Test	All
RMSE	395.50	350.83	386.43	557.75	590.42	564.86	613.12	943.98	696.80
MAE	299.45	260.48	291.16	454.22	380.69	438.58	417.55	653.71	467.80

6. Discussion

The utilization of an optimization algorithm to determine the unknown parameters of the artificial neural network model addresses the limited availability of laboratory data and the complexity of multiple input variables, ensuring accurate predictions. The sensitivity analysis conducted by the authors provides valuable insights into the influence of individual input variables on the output parameter. Identifying the sixth, eighth, and tenth variables as significant contributors allows for targeted adjustments in design and analysis. The relative importance of section length emphasizes its significance in affecting the target flexural capacity.

The authors' introduction of a step-by-step statistical approach to extract a simplified computational structure from the ANN, resulting in Equation (17), enhances the efficiency of the neural network model and simplifies the estimation of flexural strength. Furthermore, the authors' models demonstrate acceptable accuracy when compared to laboratory values and the AISC 341-16 seismic provisions, suggesting their potential as reliable tools for estimating the flexural capacity of CSW members in seismic regions.

The primary limitation is the scarcity of available laboratory data for CSWs, which constrained the size of the dataset and potentially limited the ANN predictive capabilities. As more experimental data become available, the accuracy of the models could be further improved. Additionally, the complexity of the ANN structures may pose challenges for implementation and interpretation by practitioners who are not familiar with neural networks. The authors' proposed computational approaches offer several advantages for estimating the flexural capacity of CSWs. These advantages include acceptable predictions, sensitivity analysis insights, and the introduction of a user-friendly formula.

An inherent challenge faced in this research pertains to the limited availability of laboratory data for CSWs. The dataset's size is notably constrained due to this limitation, which may affect the predictive capabilities of the artificial neural network models. It is essential to recognize that data quantity significantly influences the accuracy of predictive models. The shortage of data represents a fundamental limitation that must be considered

when applying these models in practical engineering contexts. Additionally, sensitivity analysis conducted in this research identified specific input variables, such as section length, as having a significant impact on the target flexural capacity. Nevertheless, the extent to which these findings can be extrapolated to real-world scenarios featuring diverse input data remains an open question. The authors recommend future research endeavors to address these constraints by focusing on the following areas:

- Expanding the dataset: Efforts should be directed towards collecting a more extensive dataset of laboratory data for CSWs to bolster the robustness and generalizability of predictive models.
- Real-world validation: Conducting further experiments and sensitivity analyses within real-world applications to validate the models and account for unexplored factors.

Acknowledging these limitations and pursuing research in these directions is expected to contribute to the practical applicability and reliability of these models in the field of structural engineering.

7. Conclusions

In this article, two computational approaches are introduced for estimating the flexural capacity of reinforced concrete-filled composite plate shear walls. Laboratory test results from the literature, comprising 47 datasets, are utilized with 11 input variables to evaluate the flexural behavior of the models. The findings can be summarized as follows:

- Due to limited laboratory data and the complexity of multiple variables in the problem, the number of unknown parameters in the ANN structures exceeded the available data. To overcome this, an optimization algorithm was employed to determine the unknown parameters of the model. The results indicate that a network with 28 neurons in the middle layer demonstrates good accuracy in estimating the target parameter.
- Sensitivity analysis reveals that altering the values of the steel plate thickness in the boundary element, yield strength of the steel faceplate, and concrete strength results in a decrease in the output, while changes in other variables lead to an increase in the output parameter.
- The weight values of the ANN, along with a numerical relationship, reveal that the section length has the most significant impact on the target parameter, with a relative importance value of 13.78%.
- To enhance the efficiency of the neural network model and reduce matrix calculations in estimating flexural strength, a step-by-step statistical approach was employed to extract a computational structure from the proposed ANN, resulting in the user-friendly formula of Equation (17).
- Based on the results obtained from the two proposed models in this article and their comparison with laboratory values, it is concluded that both proposed models exhibit acceptable accuracy compared to the AISC 341-16 seismic provisions. These models can be utilized for estimating the target parameter in this research, which is the flexural capacity of CSW members.

Future research should consider conducting additional experiments and sensitivity analyses to validate the models further and account for any unexplored factors that could affect the flexural capacity estimation for composite plate shear walls. This acknowledgment of limitations and the potential need for further refinement strengthens the robustness of the findings and encourages a more comprehensive exploration of this important topic.

Author Contributions: Conceptualization, M.M. and H.N.; methodology, M.M., H.N., D.-P.N.K. and T.N.N.; software, M.M. and H.N.; validation, M.M., H.N. and D.-P.N.K.; formal analysis, M.M., H.N. and D.-P.N.K.; investigation, M.M., H.N., D.-P.N.K., A.J.-G., R.J. and T.N.N.; resources, M.M., H.N., D.-P.N.K., A.J.-G., R.J. and T.N.N.; data curation, M.M., H.N. and D.-P.N.K.; writing—original draft preparation, M.M. and H.N.; writing—review and editing, D.-P.N.K., A.J.-G. and R.J.; visualization, M.M.; supervision, H.N., D.-P.N.K. and R.J.; project administration, H.N. and D.-P.N.K. All authors have read and agreed to the published version of the manuscript.

Funding: This research received no external funding.

Data Availability Statement: The data used to support the findings of this study are included within the article.

Conflicts of Interest: The authors declare no conflict of interest.

References

1. Katsikadelis, J.; Kokkinos, F. Static and dynamic analysis of composite shear walls by the boundary element method. *Acta Mech.* **1987**, *68*, 231–250. [CrossRef]
2. Yamada, M. Steel Panel encased RC composite shear walls. In Proceedings of the Composite Construction in Steel and Concrete II–Proceedings of an ASCE Engineering Foundation Conference, Trout Lodge, Potosi, MO, USA, 14–19 June 1992; pp. 899–912.
3. Ren, X.D.; Bai, Q.; Yang, C.D.; Li, J. Seismic behavior of tall buildings using steel–concrete composite columns and shear walls. *Struct. Des. Tall Spec. Build.* **2018**, *27*, e1441. [CrossRef]
4. Li, J.; Li, F.; Liu, C.; Miao, J. Numerical and theoretical analysis of seismic behaviour of CFDSP composite shear walls. *J. Build. Eng.* **2020**, *31*, 101359. [CrossRef]
5. Tran, H.; Thai, H.T.; Ngo, T.; Uy, B.; Li, D.; Mo, J. Nonlinear inelastic simulation of high-rise buildings with innovative composite coupling shear walls and CFST columns. *Struct. Des. Tall Spec. Build.* **2021**, *30*, e1883. [CrossRef]
6. Wright, H.D.; Hossain, K.M.A.; Gallocher, S.C. Composite Walls as shear elements in tall structures. In Proceedings of the ASCE Structures Congress XII, Atlanta, GA, USA, 24–28 April 1994; pp. 140–145.
7. Curkovic, I.; Skejic, D.; Dzeba, I.; Lukacevic, I. Behaviour of Composite Plate Shear Walls with Variable Column Stiffness. *ce/papers* **2021**, *4*, 754–763. [CrossRef]
8. Dong, H.; Cao, W.; Wu, H.; Zhang, J.; Xu, F. Analysis and seismic tests of composite shear walls with CFST columns and steel plate deep beams. *Earthq. Eng. Eng. Vib.* **2013**, *12*, 609–624. [CrossRef]
9. Zhao, W.; Guo, Q.; Huang, Z.; Tan, L.; Chen, J.; Ye, Y. Hysteretic model for steel–concrete composite shear walls subjected to in-plane cyclic loading. *Eng. Struct.* **2016**, *106*, 461–470. [CrossRef]
10. Kisa, M.H.; Yuksel, S.B.; Caglar, N. Experimental study on hysteric behavior of composite shear walls with steel sheets. *J. Build. Eng.* **2021**, *33*, 101570. [CrossRef]
11. Kizilarslan, E.; Broberg, M.; Shafaei, S.; Varma, A.H.; Bruneau, M. Seismic design coefficients and factors for coupled composite plate shear walls/concrete filled (CC-PSW/CF). *Eng. Struct.* **2021**, *244*, 112766. [CrossRef]
12. Nie, J.-G.; Ma, X.-W.; Tao, M.-X.; Fan, J.-S.; Bu, F.-M. Effective stiffness of composite shear wall with double plates and filled concrete. *J. Constr. Steel Res.* **2014**, *99*, 140–148. [CrossRef]
13. Yan, J.-B.; Hu, H.-T.; Wang, T. Cyclic tests on concrete-filled composite plate shear walls with enhanced C-channels. *J. Constr. Steel Res.* **2021**, *179*, 106522. [CrossRef]
14. Meftah, S.; Tounsi, A.; Megueni, A.; Bedia, E.A. Lateral stiffness and vibration characteristics of RC shear walls bonded with thin composite plates. *Compos. Struct.* **2006**, *73*, 110–119. [CrossRef]
15. Meftah, S.A.; Tounsi, A. Lateral stiffness and vibration characteristics of damaged RC coupled shear walls strengthened with thin composite plates. *Build. Environ.* **2007**, *42*, 3596–3605. [CrossRef]
16. Zhou, Y.; Lu, X.; Dong, Y. Seismic behaviour of composite shear walls with multi-embedded steel sections. Part I: Experiment. *Struct. Des. Tall Spec. Build.* **2010**, *19*, 618–636. [CrossRef]
17. Arabzadeh, A.; Soltani, M.; Ayazi, A. Experimental investigation of composite shear walls under shear loadings. *Thin-Walled Struct.* **2011**, *49*, 842–854. [CrossRef]
18. Zhang, K.; Varma, A.H.; Malushte, S.R.; Gallocher, S. Effect of shear connectors on local buckling and composite action in steel concrete composite walls. *Nucl. Eng. Des.* **2014**, *269*, 231–239. [CrossRef]
19. Yeghnem, R.; Meftah, S.; Benyoucef, S.; Tounsi, A.; Bedia, E.A. A finite-element model for the lateral stiffness and vibration characteristics of RC shear walls strengthened with composite sheets: Creep and the shrinkage effect. *Mech. Compos. Mater.* **2013**, *49*, 181–192. [CrossRef]
20. Meftah, S.; Mohri, F.; Daya, E. Seismic behavior of RC coupled shear walls with strengthened coupling beams by bonded thin composite plates. *KSCE J. Civ. Eng.* **2013**, *17*, 403–414. [CrossRef]
21. Rahnavard, R.; Hassanipour, A.; Mounesi, A. Numerical study on important parameters of composite steel-concrete shear walls. *J. Constr. Steel Res.* **2016**, *121*, 441–456. [CrossRef]
22. Shafaei, S.; Ayazi, A.; Farahbod, F. The effect of concrete panel thickness upon composite steel plate shear walls. *J. Constr. Steel Res.* **2016**, *117*, 81–90. [CrossRef]
23. Dey, S.; Bhowmick, A.K. Seismic performance of composite plate shear walls. *Structures* **2016**, *6*, 59–72. [CrossRef]
24. Mohammadgholibeyki, N.; Epackachi, S. Fragility functions for steel-plate concrete composite shear walls. *J. Constr. Steel Res.* **2020**, *167*, 105776. [CrossRef]
25. Xiao, C.; Zhu, A.; Li, J.; Li, Y. Experimental study on seismic performance of embedded steel plate-HSC composite shear walls. *J. Build. Eng.* **2021**, *34*, 101909. [CrossRef]
26. Seo, J.; Varma, A.H.; Sener, K.; Ayhan, D. Steel-plate composite (SC) walls: In-plane shear behavior, database, and design. *J. Constr. Steel Res.* **2016**, *119*, 202–215. [CrossRef]

27. Nguyen, N.H.; Whittaker, A.S. Numerical modelling of steel-plate concrete composite shear walls. *Eng. Struct.* **2017**, *150*, 1–11. [CrossRef]
28. Shafaei, S.; Farahbod, F.; Ayazi, A. The wall–frame and the steel–concrete interactions in composite shear walls. *Struct. Des. Tall Spec. Build.* **2018**, *27*, e1476. [CrossRef]
29. Wang, W.; Ren, Y.; Han, B.; Ren, T.; Liu, G.; Liang, Y. Seismic performance of corrugated steel plate concrete composite shear walls. *Struct. Des. Tall Spec. Build.* **2019**, *28*, e1564. [CrossRef]
30. Varma, A.H.; Shafaei, S.; Klemencic, R. Steel modules of composite plate shear walls: Behavior, stability, and design. *Thin-Walled Struct.* **2019**, *145*, 106384. [CrossRef]
31. Haghi, N.; Epackachi, S.; Kazemi, M.T. Macro modeling of steel-concrete composite shear walls. *Structures* **2020**, *23*, 383–406. [CrossRef]
32. Hayatdavoodi, A.; Dehghani, A.; Aslani, F.; Alahi, F.N. The development of a novel analytical model to design composite steel plate shear walls under eccentric shear. *J. Build. Eng.* **2021**, *44*, 103281. [CrossRef]
33. Kizilarslan, E.; Broberg, M.; Shafaei, S.; Varma, A.H.; Bruneau, M. Non-linear analysis models for Composite Plate Shear Walls-Concrete Filled (C-PSW/CF). *J. Constr. Steel Res.* **2021**, *184*, 106803. [CrossRef]
34. Olabi, M.N.; Caglar, N.; Kisa, M.H.; Yuksel, S.B. Numerical study on the response of composite shear walls with steel sheets under cyclic loading. *J. Build. Eng.* **2021**, *34*, 102069. [CrossRef]
35. Shafaei, S.; Varma, A.H.; Broberg, M.; Klemencic, R. Modeling the cyclic behavior of composite plate shear walls/concrete filled (C-PSW/CF). *J. Constr. Steel Res.* **2021**, *184*, 106810. [CrossRef]
36. Zhang, X.; Qin, Y.; Chen, Z. Experimental seismic behavior of innovative composite shear walls. *J. Constr. Steel Res.* **2016**, *116*, 218–232. [CrossRef]
37. Guo, L.; Rong, Q.; Qu, B.; Liu, J. Testing of steel plate shear walls with composite columns and infill plates connected to beams only. *Eng. Struct.* **2017**, *136*, 165–179. [CrossRef]
38. Wu, L.; Tian, Y.; Su, Y.; Chen, H. Seismic performance of precast composite shear walls reinforced by concrete-filled steel tubes. *Eng. Struct.* **2018**, *162*, 72–83. [CrossRef]
39. Guo, L.; Wang, Y.; Zhang, S. Experimental study of rectangular multi-partition steel-concrete composite shear walls. *Thin-Walled Struct.* **2018**, *130*, 577–592. [CrossRef]
40. Ren, F.; Chen, J.; Chen, G.; Guo, Y.; Jiang, T. Seismic behavior of composite shear walls incorporating concrete-filled steel and FRP tubes as boundary elements. *Eng. Struct.* **2018**, *168*, 405–419. [CrossRef]
41. Zhang, H.; Liu, H.; Li, G.; Ning, X. Seismic performance of encased steel plate-reinforced gangue concrete composite shear walls. *KSCE J. Civ. Eng.* **2019**, *23*, 2919–2932. [CrossRef]
42. Labibzadeh, M.; Hamidi, R. A comparison between shear capacities of two composite shear walls: DSCSWs and CSPSWs. *Struct. Eng. Int.* **2019**, *29*, 276–281. [CrossRef]
43. Zhang, W.; Wang, K.; Chen, Y.; Ding, Y. Experimental study on the seismic behaviour of composite shear walls with stiffened steel plates and infilled concrete. *Thin-Walled Struct.* **2019**, *144*, 106279. [CrossRef]
44. Zhang, J.; Li, X.; Cao, W.; Yu, C. Seismic behavior of composite shear walls incorporating high-strength materials and CFST boundary elements. *Eng. Struct.* **2020**, *220*, 110994. [CrossRef]
45. Hu, L.; Feng, P.; Lin, H.; Yang, J.-Q.; Qiang, H. Seismic performance of composite shear walls with embedded FCCCs in boundary elements. *Compos. Struct.* **2021**, *257*, 113126. [CrossRef]
46. Yan, J.-B.; Hu, H.-T.; Wang, T. Seismic behaviour of novel concrete-filled composite plate shear walls with boundary columns. *J. Constr. Steel Res.* **2021**, *179*, 106507. [CrossRef]
47. Dan, D.; Fabian, A.; Stoian, V. Nonlinear behavior of composite shear walls with vertical steel encased profiles. *Eng. Struct.* **2011**, *33*, 2794–2804. [CrossRef]
48. Booth, P.N.; Bhardwaj, S.R.; Tseng, T.-C.; Seo, J.; Varma, A.H. Ultimate shear strength of steel-plate composite (SC) walls with boundary elements. *J. Constr. Steel Res.* **2020**, *165*, 105810. [CrossRef]
49. Haghi, N.; Epackachi, S.; Kazemi, M.T. Cyclic performance of composite shear walls with boundary elements. *Structures* **2020**, *27*, 102–117. [CrossRef]
50. Wang, J.-J.; Nie, X.; Bu, F.-M.; Tao, M.-X.; Fan, J.-S. Experimental study and design method of shear-dominated composite plate shear walls. *Eng. Struct.* **2020**, *215*, 110656. [CrossRef]
51. Mei, C.; Zhao, Z.; Zhang, Y.; Wang, D.; Wu, C. Performance Evaluation and Shear Resistance of Modular Prefabricated Two-Side Connected Composite Shear Walls. *KSCE J. Civ. Eng.* **2021**, *25*, 2936–2950. [CrossRef]
52. Zhou, J.; Ling, Y.; Jiang, Y. Seismic Behaviour of PC-encased HCSC Composite Shear Walls under Vertical Tension and Horizontal Cyclic Loading. *J. Earthq. Eng.* **2022**, *26*, 6778–6802. [CrossRef]
53. Mo, J.; Uy, B.; Li, D.; Thai, H.T.; Tran, H. A review of the behaviour and design of steel–concrete composite shear walls. *Structures* **2021**, *31*, 1230–1253. [CrossRef]
54. *ANSI/AISC 341-16*; Seismic Provisions for Structural Steel Buildings. AISC: Chicago, IL, USA, 2016.
55. Nie, X.; Wang, J.-J.; Tao, M.-X.; Fan, J.-S.; Bu, F.-M. Experimental study of flexural critical reinforced concrete filled composite plate shear walls. *Eng. Struct.* **2019**, *197*, 109439. [CrossRef]
56. Hooshmand, M.K.; Hosahalli, D. Network anomaly detection using deep learning techniques. *CAAI Trans. Intell. Technol.* **2022**, *7*, 228–243. [CrossRef]

57. Yadav, K.; Yadav, M.; Saini, S. Stock values predictions using deep learning based hybrid models. *CAAI Trans. Intell. Technol.* **2022**, *7*, 107–116. [CrossRef]
58. Zhang, Z.; De Luca, G.; Archambault, B.; Chavez, J.; Rice, B. Traffic Dataset and Dynamic Routing Algorithm in Traffic Simulation. *J. Artif. Intell. Technol.* **2022**, *2*, 111–122. [CrossRef]
59. Zheng, M.; Zhi, K.; Zeng, J.; Tian, C.; You, L. A hybrid CNN for image denoising. *J. Artif. Intell. Technol.* **2022**, *2*, 93–99. [CrossRef]
60. Rumelhart, D.E.; Hinton, G.E.; Williams, R.J. Learning representations by back-propagating errors. *Nature* **1986**, *323*, 533–536. [CrossRef]
61. Mirrashid, M.; Naderpour, H. Transit search: An optimization algorithm based on exoplanet exploration. *Results Control Optim.* **2022**, *7*, 100127. [CrossRef]
62. Milne, L. Feature selection using neural networks with contribution measures. In Proceedings of the Eighth Australian Joint Conference on Artificial Intelligence, AI'95, Canberra, Australia, 13–17 November 1995.